

Observational Signatures of the First Quasars

Zoltán Haiman¹ and Abraham Loeb²

Astronomy Department, Harvard University, 60 Garden Street, Cambridge, MA 02138

ABSTRACT

We study the observational signatures of a potential population of low-luminosity quasars at high redshifts in a Λ CDM cosmology. We derive the evolution of the quasar luminosity function at fainter luminosities and higher redshifts than currently detected, based on three assumptions: (1) the formation of dark-matter halos follows the Press–Schechter theory, (2) the ratio of central black hole mass to halo mass is the same for all halos, and (3) the light-curve of quasars, in Eddington units, is universal. We show that a universal light-curve provides an excellent fit to the observed quasar luminosity function at redshifts $2.6 < z < 4.5$. By extrapolating the evolution of this luminosity function to higher redshifts ($4.5 < z < 20$), we find that the associated early population of low-luminosity quasars reionizes the universe at a redshift $z \sim 12$. The reprocessing of the UV light of these quasars by dust from early type II supernovae, distorts the microwave background spectrum by a Compton y -parameter, $y \sim 10^{-5}$, comparable to the upper limit set by COBE. The Next Generation Space Telescope could detect tens of quasars from redshifts $z > 10$ per square arcminute, with its proposed 1nJy sensitivity at 1–3.5 μ m. Absorption spectra of several such quasars would reveal the reionization history of the universe.

Subject headings: cosmology: theory – quasars: general

Submitted to *The Astrophysical Journal*

1. Introduction

One of the outstanding problems in cosmology is the nature of the first generation of astrophysical objects which appeared when the universe first transformed from its initial smooth state to its current clumpy state. Although we have observational data on bright quasars and galaxies out to redshifts $z \sim 5$ (Schneider, Schmidt & Gunn 1991; Franx et al. 1997), and on the linear density fluctuations at redshift $z \sim 10^3$ (Bennett et al. 1996), there is currently no

¹email:zhaiman@cfa.harvard.edu

²email:aloeb@cfa.harvard.edu

direct evidence as to when and how the first structures formed, and what kind of objects were responsible for end of the “dark age” of the universe (Rees 1996).

Popular Cold Dark Matter (CDM) models for structure formation predict the appearance of the first baryonic objects with masses $M \sim 10^5 M_\odot$ at redshifts as high as $z \sim 30$; objects with progressively higher masses assemble later (cf. Haiman, Thoul & Loeb, and references therein). Following virialization, the gas in these objects can only continue to collapse and fragment if it can cool on a timescale shorter than the Hubble time. In the metal-poor primordial gas, the only coolants that satisfy this requirement are neutral atomic hydrogen (H) and molecular hydrogen (H_2). However, H_2 molecules are fragile, and are easily photodissociated throughout the universe by trace amounts of starlight (Haiman, Rees, & Loeb 1996, 1997; Gnedin & Ostriker 1997). Hence, most of the first stars are expected to form inside objects with virial temperatures $T_{\text{vir}} \gtrsim 10^4 \text{K}$. Depending on the details of their cooling and angular momentum transport, the gas in these objects is expected to either fragment into stars, or form a central black hole exhibiting quasar activity. Conversion of a small fraction ($\sim 1 - 10\%$) of the gas into stars or quasars could reionize the universe, and strongly affect the entropy of the intergalactic medium.

In two previous papers (Haiman & Loeb 1997a, hereafter HL97; and Loeb & Haiman, 1997, hereafter LH97), we explored the impact of the first stars on the reionization history of the universe. In this paper, we study the related signatures of early quasars, and compare their effects to those expected from the stars. For both types of sources, we calibrate the total amount of light they produce based on data from redshifts $z \lesssim 5$. The efficiency of early star formation is calibrated based on the observed metallicity of the intergalactic medium (Songaila & Cowie 1996, Tytler et al. 1995), while the early quasars are constrained to match the quasar luminosity function at redshifts $z \lesssim 5$ (Pei 1995). In HL97 and LH97 we have studied a range of standard Cold Dark Matter (CDM) cosmologies, but in this paper we focus on a particular cosmological model with a cosmological constant, namely the “concordance model” of Ostriker & Steinhardt (1995). Within this model, we predict the number of high-redshift low-luminosity quasars using the Press–Schechter formalism (Press & Schechter 1974).

We assume that the luminosity history of each black hole depends only on its mass, and postulate the existence of a universal quasar light-curve in Eddington units. This approach is motivated by the fact that for a sufficiently high fueling rate, quasars are likely to shine at their maximum possible luminosity, which is some constant fraction of the Eddington limit, for a time which is dictated by their final mass and radiative efficiency. If the radiative efficiency were determined by a universal accretion geometry, then the bright phase of quasars would admit such a universal light-curve. We also assume that the final black hole mass is a fixed fraction of the total halo mass, and allow this fraction to be a free parameter. Based on this minimal set of assumptions, we demonstrate that there exists a universal light curve, for which the Press–Schechter theory provides an excellent fit to the observed evolution of the luminosity function of bright quasars between redshifts $2.6 < z < 4.5$. Furthermore, our fitting procedure results in black hole to halo mass ratios close to the typical values found in local galaxies

(Kormendy et al. 1997; Magorrian et al. 1997). Given this ratio and the fitted light–curve, we then extrapolate the observed LF to higher redshifts and low luminosities.

Previous work on modeling the evolution of the quasar LF has been mostly phenomenological, and involved fitting ad–hoc parametric functions to the observations (Pei 1995, Boyle et al. 1991). Small & Blandford (1992) had used a universal quasar light–curve, together with the observed LF evolution, to infer the birth–rate of quasar black holes. Haehnelt & Rees (1993; see also Efstathiou & Rees 1988) adopted the Press–Schechter theory for halo formation, specified the quasar light–curve a priori, and introduced a redshift and halo–mass dependence to the black hole formation efficiency, in order to fit the observed evolution of the quasar LF. The postulated (ad–hoc) exponential decrease in the efficiency for black hole formation in small halos (with circular velocities less than 400 km/s) could be attributed to the expulsion of gas from shallow potential wells by supernova–driven winds or mergers. However, this prescription appears to be violated in nearby low–mass galaxies, such as the compact ellipticals M32 and NGC 4486B. In particular, van der Marel et al. (1997) infer a black hole mass of $\sim 3.4 \times 10^6 M_\odot$ in M32, which is a fraction $\sim 8 \times 10^{-3}$ of the stellar mass of the galaxy, $\sim 4 \times 10^8 M_\odot$, for a central mass–to–light ratio of $\gamma_V = 2$; while Kormendy et al. (1997) infer a black hole mass of $6 \times 10^8 M_\odot$ in NGC 4486B which is a fraction $\sim 9\%$ of the stellar mass. The efficiency of black hole formation in these systems had been comparable if not higher than in galaxies with deeper potential wells. Observations of galactic nuclei in the local universe imply black hole masses which are typically a fraction $\sim 6 \times 10^{-3}$ of the total baryonic mass of their host (see summary of dynamical estimates in Fig. 5b of Magorrian et al. 1997; and the maximum ratio between a quasar luminosity and its host mass found by McLeod 1997). We therefore adopt the simplest possible assumption, namely that the black hole to halo mass ratio is constant, and *infer* the quasar light–curve from observations rather than postulate it. The actual formation process of low–luminosity quasars was addressed by Eisenstein & Loeb (1995), and Loeb (1997).

Based on the extrapolated quasar luminosity function, we quantify the effects of the first generation of low–luminosity quasars. In particular, the UV radiation produced by these quasars above the Lyman limit can lead to the reionization of the intergalactic medium (IGM), and to a number of observable signatures (Carr, Bond & Arnett 1984). First, the resulting optical depth of the universe to electron scattering at $z \lesssim 20$, τ_{es} , damps the microwave background anisotropies on scales $\lesssim 10^\circ$ (Efstathiou & Bond 1987; Kamionkowski, Spergel, & Sugiyama 1994; Hu & White 1996). The recently detected hint for a Doppler peak in ground–based microwave anisotropy experiments can already be used to set the constraint $\tau_{\text{es}} \lesssim 1$ (Scott, Silk & White 1995; Bond 1995). Future satellite experiments (such as MAP or Planck³) will be able to probe values of τ_{es} as small as a few percent if polarization data is gathered (Zaldarriaga, Spergel, & Seljak 1997). The quasar UV flux is also absorbed by intergalactic dust, and subsequent thermal emission by

³See the homepages for these experiments at <http://map.gsfc.nasa.gov> and at <http://astro.estec.esa.nl/SA-general/Projects/Cobras/cobras.html>.

this dust at longer wavelengths could introduce a substantial spectral distortion to the cosmic microwave background (CMB) radiation. Such a distortion due to population III stars have been investigated extensively in the past (Wright 1981; Adams et al. 1989; Bond, Carr & Hogan 1991; Wright et al. 1994; LH97), and its magnitude is currently constrained by COBE to have a Compton y -parameter $< 1.5 \times 10^{-5}$. Finally, direct detection of high-redshift low-luminosity quasars will be feasible with the Next Generation Space Telescope, whose proposed sensitivity in the $1\text{--}3.5\mu\text{m}$ range is $\sim 1\text{nJy}$.

The purpose of this paper is to quantify the above signatures of high-redshift low-luminosity quasars, and to compare them with those of early stars. The paper is organized as follows. In § 2, we describe the procedure used to find the universal quasar light-curve, and the resulting fits to the observed quasar LF at $z \lesssim 5$. In § 3, we calculate the reionization history of the intergalactic medium due to early quasars, and compare it to stellar reionization. In § 4, we discuss the effects of the early quasars on the CMB, including the smoothing of its anisotropies and the distortion of its spectrum. In § 5, we predict the number counts of high-redshift quasars down to the sensitivity limit of the Next Generation Space Telescope. Finally, § 6 summarizes the main conclusions and implications of this work.

2. Quasar Light-Curve

Our goal is to calculate the quasar luminosity function at faint magnitudes, ($\log(L_{\text{B}}/L_{\text{B},\odot}) \lesssim 11.5$) and at high redshifts ($z \gtrsim 4.5$), outside the regime of current observations. For this purpose, we introduce a new model which extrapolates the observed LF of bright quasars at redshifts $2.6 < z < 4.5$, based on the Press-Schechter theory and the assumption that all quasars admit the same universal light-curve in Eddington units.

The formation rate of dark-matter halos is given by the Press-Schechter formalism. We assume that black hole formation is restricted to halos whose virial temperature exceeds $T_{\text{vir}} \gtrsim 10^4\text{K}$, in which atomic and Bremsstrahlung cooling allows the gas to sink to the center of the potential well. This virial temperature threshold corresponds to a minimum halo mass $M_{\text{halo}} \gtrsim M_{\text{min}} = 10^8 M_{\odot} [(1+z)/10]^{-3/2}$. We further assume for simplicity that the ratio of final black hole mass to halo mass, $\epsilon \equiv M_{\text{bh}}/M_{\text{halo}}$ is the same for all halos. Estimates of black hole masses in nearby galaxies (Kormendy et al. 1997; Magorrian et al. 1997) imply that massive black holes weigh roughly a fixed fraction of their bulge mass, over a wide range of bulge masses $10^9 M_{\odot} \lesssim M_{\text{bulge}} \lesssim 2 \times 10^{12} M_{\odot}$. Since bulges are the oldest stellar components of galaxies, it is reasonable to assume that a fixed fraction of the baryonic content of early galaxies ends up in the central black hole. Note, however, that this assumption differs from the model presented by Haehnelt & Rees (1993), in which ϵ is assumed to decline exponentially for low-mass galaxies.

The change in the comoving number density of black holes with masses between M_{bh} and

$M_{\text{bh}} + dM_{\text{bh}}$, between redshifts z and $z + dz$, is governed by the derivative,

$$\left. \frac{d^2 N_{\text{bh}}(M_{\text{bh}}, z)}{dM_{\text{bh}} dz} \right|_{M_{\text{bh}}} = \begin{cases} \frac{1}{\epsilon} \frac{d}{dz} \frac{dN_{\text{ps}}(M, z)}{dM} \Big|_{M=\epsilon^{-1} M_{\text{bh}}} & (\text{for } M_{\text{bh}} \geq \epsilon M_{\text{min}}) \\ 0 & (\text{for } M_{\text{bh}} < \epsilon M_{\text{min}}), \end{cases} \quad (1)$$

where dN_{ps}/dM is the Press-Schechter mass function. The actual halo formation rate is larger than the derivative $\frac{d}{dz}(dN_{\text{ps}}/dM)$, since this derivative includes a negative contribution from merging halos. However, at high redshifts collapsed objects are rare, and the merger probability is low. We have compared the above expression with the more accurate result for the halo formation rate given by Sasaki (1994), and confirmed that the difference in the rates is negligible for the high redshifts and halo masses under consideration here. We therefore use equation (1) to describe the black hole formation rate at high redshifts.

We define $\phi(L, z)dL$ to be the number of quasars per unit comoving volume at redshift z , with intrinsic luminosities between L and $L + dL$. The luminosity function, $\phi(L, z)$, is linked to the black hole formation rate through the light-curves of the quasars. For simplicity, we make the minimal assumption that all quasars admit the same light-curve in Eddington units, i.e. their luminosity is proportional to their final mass (see §1). Under this assumption, the luminosity $L(t)$ of a quasar with a black hole mass M_{bh} at a time t after its birth can be written as

$$L(t) = M_{\text{bh}} f(t) = \epsilon M_{\text{halo}} f(t), \quad (M_{\text{halo}} > M_{\text{min}}) \quad (2)$$

where $f(t)$ is a function of time. This leads to the expression for the LF,

$$\phi(L, z) = \int_z^\infty \int_{\epsilon M_{\text{min}}}^\infty dM_{\text{bh}} dz' \frac{d^2 N_{\text{bh}}}{dM_{\text{bh}} dz'} \delta[L - M_{\text{bh}} f(t_{z, z'})], \quad (3)$$

where $t_{z, z'}$ is the time elapsed between the redshifts z and z' . By integrating over z' , we obtain

$$\phi(L, z) = \int_{\epsilon M_{\text{min}}}^\infty \frac{dM_{\text{bh}}}{M_{\text{bh}}} \frac{d^2 N_{\text{bh}}}{dM_{\text{bh}} dz} \Big|_{z_\star} \frac{dz}{dt} \Big|_{z_\star}, \quad (4)$$

or, equivalently, by integrating over M_{bh} we get,

$$\phi(L, z) = \int_0^{t(z)} \frac{dt}{f(t)} \frac{dz}{dt} \Big|_t \frac{d^2 N_{\text{bh}}}{dM_{\text{bh}} dz} \Big|_{M_{\text{bh}} = \frac{L}{f(t)}}, \quad (5)$$

where $\dot{f} = df/dt$, t_\star is defined by the condition $M_{\text{bh}} f(t_\star) \equiv L$, and z_\star is defined through the relation $t_\star \equiv t(z) - t(z_\star)$. We found it useful to utilize both of the above expressions for $\phi(L, z)$, since a comparison between them can be used to check for the numerical accuracy of the calculation. The only unknown quantities are \dot{f} in equation (4), and f in equation (5). Therefore, either of these two equations can be solved to find the $f(t)$ that would fit best the observational data. Since the equations are implicit, we have found their solution iteratively. We have optimized our initial guess for $f(t)$ as follows.

The function $d^2N_{\text{bh}}/dM_{\text{bh}}dz$ peaks at a mass scale $M_{\text{pk}} = \epsilon M_{\text{nl}}(z)$, where $M_{\text{nl}}(z)$ is the non-linear mass-scale at the corresponding redshift. Assuming that this function is sharply peaked around M_{pk} , i.e. substituting $d^2N_{\text{bh}}/dM_{\text{bh}}dz \propto \delta(M_{\text{pk}}[z])$ into equation (4), yields

$$\phi(L, z) \propto \frac{1}{M_{\text{pk}}|f|} \propto \frac{1}{|dL/dt|}, \quad (6)$$

or

$$t \propto \int_L^\infty \phi(L', z) dL'. \quad (7)$$

In the last step, we assumed that $dL/dt < 0$, i.e. that the quasar’s luminosity decreases monotonically with time. Equation (7) yields the time t it takes the quasar luminosity to drop down to $L = M_{\text{pk}}f$, and provides a “first guess” solution for $t(f)$ and hence for $f(t)$. The physical interpretation of the LF in this case is that it merely reflects the time spent by the quasars in each luminosity interval.

To find the light-curve $f(t)$, we need to specify $\phi(L, z)$. Given the observational data, the inferred luminosity function depends on the assumed cosmology and quasar spectrum (the latter due to k -corrections). In this paper, we adopt the “concordance model” of cosmological parameters highlighted by Ostriker & Steinhardt (1995), i.e. a flat Λ CDM model with a slightly tilted power spectrum $(\Omega_{\text{m}}, \Omega_{\Lambda}, \Omega_{\text{b}}, h, \sigma_{8h^{-1}}, n) = (0.35, 0.65, 0.04, 0.65, 0.87, 0.96)$. Convenient expressions in this model for the differential volume element, luminosity distance, and time-redshift relation were given in terms of elliptic integrals by Eisenstein (1997). An accurate arithmetic fitting formula for the growth function that appears in the Press-Schechter formula, is given by Carroll et al. (1992). For the average quasar spectrum, we have used the “median” spectrum derived from observed spectra of 47 quasars by Elvis et al. (1994). This spectrum is shown in Figure 1.

Pei (1995) provides a fitting formula for the B-band ($0.44 \mu\text{m}$ rest-wavelength) luminosity function of observed quasars, $\phi(L_{\text{B}}, z)$, including the redshift evolution both for a flat and an open $\Omega_{\text{tot}} = 0.2$ cosmology. For conversion to Eddington units, we note that a $1M_{\odot}$ black hole, shining at Eddington luminosity with the median flux distribution of Elvis et al. (1994), has a B-band luminosity of 5.7×10^3 times the solar B-band luminosity. Pei (1995) assumes power-law spectra for the quasars, with a slope $\alpha=0.5$ in the flat model, and $\alpha=1.0$ in the open model. Since near the B-band the Elvis et al. (1994) template spectrum is very close to an $\alpha=1$ power-law, we used the open-universe fitting formulas from Pei (1995), with a rescaling of the luminosities and volume elements for our Λ CDM cosmology. Note that the exact conversion of the intrinsic LF to a different cosmology would require a spectrum-dependent k -correction, as well as rescaling the luminosity and the volume element, for the redshift of each individual quasar. However, we have found that using the mean redshift in each redshift bin, and assuming the $\alpha=1.0$ power-law for our quasar spectrum, provided the correct LF to within several percent.

Figure 2 shows the resulting fitting formulas for $\phi(L_{\text{B}}, z)$, together with the observational data points for the LF, in the Λ CDM cosmology at redshifts $z=2.6, 3$, and 4. Using the fitting formula derived by Pei (1995), equation (7) yields an initial guess for $f(t)$. The numerical solution for this

guess can be fitted by a parameterized function, and substituted back into equation (4) or (5). The parameters of the fit can then be iteratively adjusted so as to optimize the match between the resulting $\phi(L, z)$ and the observed quasar LF at $z = 2.6, 3$, and 4. Using this procedure, we have found that an excellent fit is achieved through a simple single-parameter function for the light-curve,

$$f(t) = \frac{L_{\text{Edd}}}{M_{\text{bh}}} \exp\left(-\frac{t}{t_0}\right), \quad (8)$$

where $L_{\text{Edd}} \equiv 1.4 \times 10^{38} \text{ erg s}^{-1} (M_{\text{bh}}/M_{\odot})$ is the Eddington luminosity for the final⁴ black hole mass M_{bh} . Our model, therefore, has only two free parameters, t_0 and ϵ . The best fit values of these parameters are $t_0 = 10^{5.82} \text{ yr}$ and $\epsilon = 10^{-3.2}$. The best-fit light-curve is shown in Figure 3, while the resulting luminosity functions at $z = 2.6, 3$, and 4, are shown by the solid lines in Figure 2.

Our procedure results in fits to the LF comparable in quality to the original ad-hoc parametric fits given by Pei (1995). It is rather remarkable that, in the range of observed luminosities, the two curves are almost indistinguishable, even though at fainter magnitudes our curves deviate from the Pei (1995) fits, and predict many more quasars than the extrapolation of those fitting formulae. Another gratifying feature of our approach is that – with the underlying assumption that the flat portion of the light-curve corresponds to the Eddington luminosity limit of the final black hole – it results in a prediction for the black hole to halo mass, $M_{\text{bh}}/M_{\text{halo}} = 10^{-3.2}$, or black hole to gas mass $M_{\text{bh}}/M_{\text{gas}} = 10^{-3.2} \Omega_{\text{m}}/\Omega_{\text{b}} = 5.4 \times 10^{-3}$. This is close to the value derived from observational data, 6×10^{-3} , for the bulges of nearby galaxies (Kormendy et al. 1997; Magorrian et al. 1997), which might have formed at about the same time as quasars. There are, however, two shortcomings of our model. First, since it is based on the Press-Schechter formalism, it predicts that the number of bright quasars (those with masses above M_{pk} , or $L_{\text{B}} \gtrsim 10^{13} L_{\text{B},\odot}$) is steadily increasing down to $z = 0$. Hence, by construction, it cannot explain the decrease in the number density of bright quasars at low redshifts ($z \lesssim 2$). This decrease might be associated with the decline in merger rates at low redshifts (Carlberg 1990); or it might also be a result of the expulsion of cold gas from galaxies through supernovae-driven winds due to the peak in the star formation activity around $z \sim 2$ (Madau 1997). However, since our predictions focus on high redshifts ($z \gtrsim 5$), we ignore this shortcoming of the model. Second, the best-fit light-curve predicts a quasar lifetime of only $\sim 6.6 \times 10^5$ years, about two orders of magnitude shorter than the Eddington time at the usually assumed value of the radiative efficiency, 10%. The average radiative efficiency over the growth history of the black hole, is $\sim 0.1\%$, two orders of magnitude smaller than the value for thin disks (Frank et al. 1992). This may imply that quasar black holes accumulate most of their mass in an accretion flow with a low radiative efficiency, such as

⁴During the initial growth of the black hole, its mass and hence its Eddington limit, are smaller. This is not in conflict with our prescribed light-curve, as long as most of the light is emitted during a late phase of duration t_0 , during which the black hole shines close to the Eddington limit of its final mass, M_{bh} . The inferred low value of t_0 implies that much of the black hole mass is accumulated via accretion with a low radiative efficiency (e.g., an advection-dominated accretion flow, cf. Narayan 1996 and references therein).

advection dominated flows (Narayan 1996, and references therein). Although t_0 is an unusually short lifetime for the bright phase of quasars, it is not in conflict with existing observations. Furthermore, increasing the lifetime of quasars would enhance all of the effects that we describe below. In this sense, we are being conservative by adopting our best-fit light-curve.

The evolution predicted by equation (5) for the quasar LF between redshifts $2.6 < z < 18$, is shown in Figure 4. The break at $L_B \sim 10^{10} L_{B,\odot}$ is introduced by our imposed low-mass cutoff $M_{\text{halo}} \geq 10^8 M_\odot [(1+z)/10]^{-3/2}$. In Figure 5, we show the evolution of the number density of quasars brighter than absolute blue magnitude $M_B = -27.5$ and -22.5 ($L_B = 10^{13.2} L_{B,\odot}$ and $10^{11.2} L_{B,\odot}$, respectively). The solid lines in this figure show the number densities predicted by our model, while the dotted lines show the corresponding number densities based on Pei’s (1995) fitting formulas. This figure demonstrates that although our model agrees with the observational data between $2.6 < z < 4.5$, it predicts a substantially larger abundance of quasars at higher redshifts and fainter magnitudes, than the formal extrapolations of the fitting formulae given by Pei (1995).

3. Reionization

In this section, we derive the reionization history of the IGM in the presence of early quasars. The method of calculation follows closely the one introduced in HL97 for the case of stellar reionization. We refer the reader to this reference for more details.

Each ionizing source creates an expanding Strömgen sphere around itself. Reionization is complete when the separate HII regions overlap (Arons & Wingert 1972). Since the neutral fraction inside each HII region is small ($\sim 10^{-6}$) and the mass-weighted clumpiness of the IGM is still small at $z \gtrsim 10$ (Gnedin & Ostriker 1997), the average ionized fraction at any redshift is simply given by the filling factor of the HII regions. The reionization history depends on the formation rate of quasars, the light-curve of ionizing photons from quasars, and the recombination rate in the IGM, which are all functions of redshift.

The production rate of ionizing photons per quasar follows from the quasar spectrum and light-curve shown in Figures 1 and 3. The production rate per solar mass of the black hole, $dN_{E>13.6\text{eV}}/dt = 6.6 \times 10^{47} M_{\text{bh}} f(t) \text{ photons } M_\odot^{-1} \text{ s}^{-1}$, is shown as the solid line in Figure 6. For comparison, we also show the analogous rate per stellar mass from the composite stellar spectrum in our model of a zero-metallicity starburst. Note that although the quasar rate is initially higher than the stellar rate by two orders of magnitude, it drops much more rapidly at later times. The total number of ionizing photons produced by a quasar is $\sim 1.3 \times 10^{61} M_{\text{bh}}/M_\odot$, only an order of magnitude higher than that of stars, $\sim 1.3 \times 10^{60} M_{\text{stars}}/M_\odot$.

We assume that recombinations take place only in the homogeneous IGM. This includes the implicit assumption that all of the ionizing photons escape from the neighborhood of the quasar. While this would be a poor assumption for stellar radiation, it is justified for the much more

intense (and harder) quasar emission. A simple estimate can be used to show that the quasar host would be ionized shortly after the quasar turns on. Indeed, the known quasars do not show any sign of associated (galactic) HI absorption in their spectrum, while stellar spectra of high redshift galaxies often do. An additional assumption in obtaining the recombination rate is that the IGM is homogeneous, i.e. the clumping factor for ionized hydrogen is unity, $C_{\text{HII}} \equiv \langle n_{\text{HII}}^2 \rangle / \langle n_{\text{HII}} \rangle^2 = 1$. This is justified in numerical simulations, which show that C_{HII} rises significantly above unity only when the collapsed fraction of baryons is large, i.e. at $z \lesssim 10$ (see Fig. 2 in Gnedin & Ostriker 1997)

The evolution of a cosmological ionization front for a time-dependent source is governed by the equation,

$$n_{\text{H}} \left(\frac{dr_i}{dt} - H(t)r_i \right) = \frac{1}{4\pi r_i^2} \left(\frac{dN_\gamma}{dt}(t) - \frac{4}{3}\pi r_i^3 \alpha_{\text{B}} n_{\text{H}}^2 \right), \quad (9)$$

where n_{H} is the neutral hydrogen number density in the IGM, r_i is the physical (i.e. not comoving) radius of the ionization front, $H(t)$ is the Hubble expansion rate at cosmic time t , dN_γ/dt is the ionizing photon rate, and $\alpha_{\text{B}} = 2.6 \times 10^{-13} \text{ cm}^3 \text{ s}^{-1}$ is the recombination coefficient of neutral hydrogen at $T = 10^4 \text{ K}$ (see HL97, or Shapiro & Giroux 1987 for more details). The solution of this equation yields the ionized volume per source, $4/3\pi r_i^3$. A summation over all sources provides the total ionized volume within the IGM.

The results for the stellar case depend on the assumed star formation efficiency, which we normalize based on the observed metallicity of the IGM at $z \sim 3$ (HL97). In individual Ly α clouds with $N_{\text{HI}} \gtrsim 10^{14} \text{ cm}^{-2}$, where C and/or Si are detected, the inferred metallicities (in solar units) are $\sim 10^{-2.5}$ for C, and $\sim 10^{-2}$ for Si (Songaila & Cowie 1996, Tytler et al. 1995). There appears to be no trend of a decreasing mean C/H or Si/H with decreasing column density, across six orders of magnitude in N_{HI} . Hence, a plausible assumption is that the metals are universally mixed into the IGM prior to $z = 3$, so that the metallicities of the low column density absorbers are the same as that found in systems with $N_{\text{HI}} \gtrsim 10^{14} \text{ cm}^{-2}$. However, as pointed out by Songaila (1997), it is also possible that there are no metals in the low column density systems; in that case, a conservative lower limit for the average metallicity is $Z_{\text{IGM}} = 10^{-3} Z_{\odot}$. The resulting range of IGM metallicities, $10^{-3} < (Z_{\text{IGM}}/Z_{\odot}) < 10^{-2}$, translates to the corresponding range $0.017 < f_{\text{star}} \equiv M_{\text{star}}/M_{\text{gas}} < 0.17$ for the star formation efficiency.

Figure 7 summarizes the resulting reionization histories of stars or quasars in our Λ CDM cosmology. The results for stars are shown in two cases, one with $Z_{\text{IGM}} = 10^{-2} Z_{\odot}$ and the other with $Z_{\text{IGM}} = 10^{-3} Z_{\odot}$, to bracket the metallicity range mentioned above. The assumed IGM metallicity does not affect the quasar calculation. The upper left panel of Figure 7 shows the fraction of baryons which reside in collapsed objects with a mass above $M_{\text{min}} = 10^8 M_{\odot} [(1+z)/10]^{-3/2}$. The upper right panel shows the evolution of the average flux, J_{21} , at the local Lyman limit frequency, in units of $10^{-21} \text{ erg s}^{-1} \text{ cm}^{-2} \text{ Hz}^{-1} \text{ sr}^{-1}$ for quasars (solid line) and stars (dashed line for $Z_{\text{IGM}} = 10^{-2} Z_{\odot}$; and dotted line for $Z_{\text{IGM}} = 10^{-3} Z_{\odot}$). The equations used to obtain J_{21} are the same as described in LH97, except for the changes in the line

element, time–redshift relation, and baryonic collapsed fraction, caused by our switch to a Λ CDM cosmology. The stellar mass function is taken to have the Scalo (1986) form. We have assumed that the flux between the local Ly α and Lyman–limit frequencies vanishes before reionization, due to the large Gunn–Peterson optical depth. Although this is a good approximation for the present purpose, we note that the actual spectrum in this frequency range is expected to have a sawtooth shape, as described in Haiman, Rees & Loeb (1997). After reionization J_{21} rises rapidly, and by a redshift $z = 3$ the stellar J_{21} reaches a value in the range 0.04–0.4, while quasars contribute $J_{21} \approx 0.1$. These values are consistent with the background flux level inferred from the proximity effect around quasars (Bechtold 1994).

The lower left panel of Figure 7 shows the resulting evolution of the ionized fraction of hydrogen, F_{HII} . The dashed curves indicate that for the high end of the allowed metallicity range, stars ionize the IGM by a redshift $z \sim 13$; while the dotted curve shows that for the lowest metallicity, reionization is delayed until $z = 9$. (Note that for $Z_{\text{IGM}} = 0.01Z_{\odot}$, HL97 obtained stellar reionization at a redshift $z = 18$ in standard CDM. The change to $z = 13$ here results from our switch to a Λ CDM cosmology.) The solid curve shows that quasars reionize the IGM between these two redshifts, at $z = 11.5$. This result can be understood simply in terms of the total number of ionizing photons produced in each case per unit halo mass: the relative ratios of this number in the three cases are $1 \div 0.37 \div 0.1$, respectively.

Although the reionization redshift can be inferred from the corresponding damping of CMB anisotropies (see below), it is not possible to determine whether reionization was caused by stars or quasars, based on the measurement of this damping alone. However, the distinction between the two possibilities could be made if the reionization redshift of HeII is also measured. If a source at a redshift prior to reionization is discovered, the location of the Gunn–Peterson trough in its spectrum would yield the reionization redshift, while the shape of the damping wing of the trough can be used to infer the Gunn–Peterson optical depth (Miralda-Escudé 1997). Since the ionization threshold of HeII is four times higher than that of HI, the ionization of HeII requires a much harder spectrum. The relevant measure is $\eta \equiv (dN_{E>54.4\text{eV}}/dt)/(dN_{E>13.6\text{eV}}/dt)$, the ratio of photon fluxes above 54.4eV and 13.6eV. Equation (9) reveals that if recombinations are negligible, and if $\eta \leq n_{\text{He}}/n_{\text{H}} \approx 0.08$, then the HeII/HeIII ionization front will lag behind the HI/HII-ionization front (see Miralda-Escudé & Rees 1994, for a discussion). If recombinations are important (redshifts $z \gtrsim 15$), then the lag is increased further, since HeII recombines 5.5 times faster than HI. In our models, the HeII reionization history can be evaluated by replacing n_{H} with n_{He} , and $dN_{E>13.6\text{eV}}/dt$ with $dN_{E>54.4\text{eV}}/dt$, and multiplying α_{B} by a factor of 5.5, in equation (9).

We find that for our quasar spectrum, HI and HeII reionization occurs almost simultaneously (the HeII reionization redshift is $z = 11.8$), but for our stellar spectrum, HeII reionization is never achieved. These results are explained by fact that for the quasar spectral template of Elvis et al. (1994), $\eta = 0.09$; while for the stellar spectral template, $\eta \sim 10^{-6}$, i.e. there are almost no HeII–ionizing photons, because most of these photons are absorbed already in the stellar

atmospheres (see Fig. 3 in HL97). It therefore seems likely that intergalactic HeII was reionized by quasars rather than by stars. Thus, the reionization history of HeII provides an ideal probe for the formation history of the first quasars.

Our results indicate that the reionization redshifts of HI and HeII should not be very different, unless we have substantially overestimated the emission from high-redshift quasars, or underestimated the abundance of high mass stars. Reimers et al. (1997) have recently claimed a detection of the HeII reionization epoch at $z = 3$. Their claim is based on the lack of any detected flux above the redshifted HeII Ly α frequency, although the flux at the corresponding redshifted HI Ly α frequencies is transmitted without any absorption. This observation, however, only places the limit $\tau_{\text{He}} \gtrsim \text{few}$ on the HeII Gunn–Peterson optical depth, rather than the $\tau_{\text{He}} \gtrsim \text{few thousand}$, required to prove HeII reionization. In fact, Miralda–Escudé (1997) argued that these observational results are likely to have been caused by spatial variations in the gas density, and fluctuations of the background radiation intensity above the HeII edge, rather than the fact that the HeIII bubbles have not yet overlapped. In summary, the interpretation of this, and other recent detections of HeII absorption (Jacobsen et al. 1994; Tytler et al. 1995; Davidsen et al. 1996; Hogan et al 1997) are still controversial, in that these measurements are consistent with the absorption arising either from non-overlapping HeIII bubbles, or from other effects associated with intervening discrete systems (see, e.g. Madau & Meiksin 1994; Giroux & Shull 1997).

4. Signatures Imprinted on the Cosmic Microwave Background

Reionization results in a reduction of the temperature anisotropies of the cosmic microwave background (CMB). The free electrons released during this epoch increase the optical depth of the universe to electron scattering (τ_{es}), and damp the CMB anisotropies on scales below the size of the horizon at that time, $\lesssim 10^\circ$ (Efstathiou & Bond 1987; Kamionkowski, Spergel, & Sugiyama 1994). The electron scattering optical depth in our models is approximately $\tau_{\text{es}}(z) \approx 0.053\Omega_b h \int dz \sqrt{1+z} F_{\text{HII}}(z)$, where $F_{\text{HII}}(z)$ is the filling factor of the HII regions. Hu & White (1997) provide a fitting formula for the damping factor of the CMB power-spectrum, R_ℓ^2 , as a function of the index ℓ in the spherical harmonic decomposition of the microwave sky [the angular scale corresponding to a given ℓ -mode is $\sim 1^\circ \times (\ell/200)^{-1}$]. The damping factor is uniquely related to the evolution of the optical depth for electron scattering as a function of redshift.

The lower right panel of Figure 7 shows both $\tau_{\text{es}}(z)$ and R_ℓ^2 for the stellar and quasar reionization histories. The electron scattering optical depth is 3–5% for the stellar case, and $\sim 4\%$ for the quasar case. The corresponding damping factors for the power spectrum of CMB anisotropies are 6–10%, and $\sim 8\%$, respectively. Although the amplitude of these damping factors is small, they are within the proposed sensitivities of the future MAP and Planck satellite experiments, if data on both temperature and polarization anisotropies of the CMB will be gathered (see Table 2 in Zaldarriaga et al. 1997).

The UV emission from early quasars could also distort the spectrum of the CMB, after being reprocessed by dust. An early epoch of star formation and metal enrichment is inevitably accompanied by the formation of dust in supernova shells. This dust would absorb the UV flux from both stars and quasars, and re-emit it at longer wavelengths. The re-emitted radiation is added to the CMB spectrum, and introduces a deviation from its perfect blackbody shape. A distortion of this type due to population III stars alone has been considered by several authors (Wright et al. 1994; Bond, Carr & Hogan 1991; Adams et al. 1989; Wright 1981).

In a previous paper (LH97), we have calculated the distortion amplitude from early stars in a standard CDM cosmology, using the Press-Schechter formalism and normalizing the star formation efficiency in collapsed objects based on the observed metallicity of the IGM. The essential assumptions in this calculation were: (1) the initial mass function (IMF) of stars at high-redshifts is the same as observed locally (Scalo 1986), and (2) each type II supernova yields $0.3M_{\odot}$ of dust, which gets uniformly distributed within the intergalactic medium. We further assumed that the dust is in thermal equilibrium with the total (CMB + stellar) radiation field, that its absorption follows the wavelength-dependent opacity of Galactic dust (Mathis 1990), and that it radiates as a blackbody at its equilibrium temperature. We have found that allowing two dust components made of graphite and silicate (Draine & Lee 1984) with independent equilibrium temperatures, does not change our results by more than a few percent. For a range of possible parameter values within standard CDM, we found that the opacity of intergalactic dust to infrared sources at redshifts $z \gtrsim 10$ is significant, $\tau_{\text{dust}} = (0.1-1)$, and that this dust distorts the microwave background spectrum by a Compton y -parameter in the range $(0.06-6) \times 10^{-5}$.

Here, we repeat the LH97 calculations in a Λ CDM cosmology, and extend them by adding the UV flux from quasars to the total radiation field. Our new results are presented in Figure 8. The top panel of this figure shows the resulting total spectrum of the radiation background (CMB + direct stellar and quasar emission + dust emission) at $z = 3$. The spectrum describes a minimum level of CMB distortion down to $z = 3$; more distortion could be added between $0 < z < 3$ by dust and radiation from galaxies. However, the additional emission at $0 < z < 3$ does not relate directly to the reionization epoch and is therefore ignored here. The dashed lines show the spectrum for the stellar case, for $Z_{\text{IGM}} = 10^{-2}Z_{\odot}$ (top curve) and $Z_{\text{IGM}} = 10^{-3}Z_{\odot}$ (bottom curve). The pronounced peak at a wavelength of $\sim 1\mu\text{m}$ is the sum of the direct starlight from high- z stars, redshifted to $z = 3$. The deviation from the pure $T_{\text{CMB}} = 2.728(1+z)\text{K}$ blackbody shape (shown by the dotted curve) are visible in this figure below a wavelength of 0.02cm . The corresponding distortions in the COBE range is quantified by the Compton y -parameter, defined as

$$y_c \equiv \frac{1}{4} \left[\frac{\int d\nu N_{\nu}}{\int d\nu N_{0,\nu}} - 1 \right], \quad (10)$$

where the integrals are evaluated over the FIRAS frequency range of 60–600 GHz (Fixsen et al. 1996), N_{ν} is the comoving number density of photons with a comoving frequency ν in the total

radiation field, and $N_{0,\nu}$ reflects the unperturbed CMB,

$$N_{0,\nu} \equiv \frac{8\pi}{c^3} \frac{\nu^3}{\exp(h\nu/k_B T_{\text{CMB}}) - 1}. \quad (11)$$

The bottom panel of Figure 8 shows the redshift evolution of the y -parameter, as well as the dust temperature, T_{dust} . For the stellar cases considered above, we obtain $1.3 \times 10^{-7} < y_c < 1.2 \times 10^{-5}$ at $z = 3$ (dashed lines). Since both the dust opacity and the stellar radiation background are independently proportional to the star-formation efficiency f_{star} , the spectral distortion is proportional to f_{star}^2 (see LH97). For the high end of the allowed metallicity range, the distortion at $z = 3$ is just below the upper limit set by COBE, $y = 1.5 \times 10^{-5}$ (Fixsen et al. 1996); for lower metallicities, the y -parameter drops rapidly below this value. The dust temperature remains in all cases close to the CMB temperature (shown by the dotted line).

The solid lines in Figure 8 show how these results change when the radiation from the early quasars is added. In particular, the top panel shows that the broad emission spectrum of quasars (cf. Fig. 1) adds a background radiation field over a much broader range of wavelengths than stellar emission. But since dust is effective in absorbing the quasar flux only in a relatively narrow range around $\sim 1\mu\text{m}$, the distortion in the COBE regime is not significantly altered. In particular, we find $4.1 \times 10^{-6} < y_c < 2.0 \times 10^{-5}$ at $z = 3$ for the range $10^{-3}Z_{\odot} < Z_{\text{IGM}} < 10^{-3}Z_{\odot}$. It is interesting to note that the long-wavelength emission from high redshift quasars in the COBE wavelength range, results in a minimum distortion of $y_c \approx 3.4 \times 10^{-6}$. Depending on Z_{IGM} , this amounts to a fraction ~ 17 – 82% of the total y -parameter values quoted before. This minimal level of distortion results simply from the cumulative far-infrared flux of early quasars, and should be present even in the absence of any intergalactic dust. It can be avoided only if early quasars have much less emission longward of $\sim 100\mu\text{m}$, relative to the spectrum shown in Figure 1.

5. Number Counts of Faint Quasars

Next we examine the feasibility of direct detection of the early population of low-luminosity quasars. Although any such detection is beyond the sensitivities of current observing programs, future instruments such as the Space Infrared Telescope Facility (SIRTF) or the Next Generation Space Telescope (NGST), will achieve the required sensitivity. NGST, which is scheduled for launch a decade from now, is expected to reach a sensitivity of ~ 1 nJy in the wavelength range 1 – $3.5\mu\text{m}$ (Mather & Stockman 1996; see also <http://ngst.gsfc.nasa.gov>). The number of sources that NGST would detect at redshifts $z > z_{\text{min}}$, per unit solid angle, with observed flux between F_{ν} and $F_{\nu} + dF_{\nu}$ (averaged over the observed wavelength range 1 – $3.5\mu\text{m}$), is given by

$$\frac{dN}{d\Omega dF_{\nu}}(F_{\nu}, z_{\text{min}}) = \int_{z_{\text{min}}}^{\infty} dz \left(\frac{dV_c}{dz d\Omega} \right) n_c(z, F_{\nu}), \quad (12)$$

where $dV_c/dz d\Omega$ is the comoving volume element per unit redshift per unit solid angle, and $n_c(z, F_{\nu})$ is the comoving number density of objects at redshift z , whose flux at $z = 0$ is observed

to be between F_ν and $F_\nu + dF_\nu$. Based on the halo formation rate $d^2N_{\text{ps}}/dMdz$ [cf. Eq. (1)], n_c is given by a sum over halos of different ages that exist at each redshift,

$$n_c(z, F_\nu) = \int_z^\infty dz' \frac{dM}{dF_\nu}(z, z', F_\nu) \left. \frac{d^2N_{\text{ps}}}{dMdz'} \right|_{M(z, z', F_\nu), z'}, \quad (13)$$

where the factor dM/dF_ν converts the number density per unit mass interval to number density per unit flux interval, based on equation (14). The assumptions implicit in this expression are that the simple derivative $d^2N_{\text{ps}}/dMdz$ gives the halo formation rate [see discussion following eq. (1)], and that the halos do not grow in mass during the active phase of the emission sources they host (a good assumption for the short-lived quasar activity). Relaxing any of these assumptions would increase our predicted number counts. Note that, in HL97 we had effectively identified $z = z'$ in the kernel of equation (13), when estimating the number counts of star clusters. This might be justified only for stellar sources that live for a Hubble time or longer. However, in this case there is a danger of double counting merging halos in neighboring redshift bins (although at sufficiently high redshifts objects are exponentially rare and their merging probability is small). We intend to address this issue more rigorously using the excursion-set formalism (Bond et al. 1991; Lacey & Cole 1993, 1994), in a future publication.

The average flux $F_\nu(z, M)$ from a halo at redshift z with mass M , that was formed at $z' \geq z$ equals

$$F_\nu(z, z') = \frac{10^{32}}{d_L(z)^2} \frac{\epsilon M}{\Delta\nu_0} \int_{\nu_{\min}}^{\nu_{\max}} d\nu j(\nu, t_{z, z'}) \quad \text{nJy}. \quad (14)$$

Here the halo mass M is in units of M_\odot ; ν_{\min} and ν_{\max} are the redshifted frequencies (in units of Hz) corresponding to the observed wavelengths of $3.5\mu\text{m}$ and $1\mu\text{m}$, respectively; $\Delta\nu_0 = 2.14 \times 10^{14}$ Hz is the width of the NGST frequency band; $d_L(z)$ is the luminosity distance in cm; $\epsilon = 10^{-3.2}$ for quasars or $\epsilon = 0.17\Omega_b/\Omega_m = 0.02$ for stars, is the fraction of halo mass in the form of the central black hole or stars, respectively; $j(\nu, t_{z, z'})$ is the template luminosity per unit (stellar or black hole) mass for either stars or quasars, in units of $\text{erg sec}^{-1} \text{ Hz}^{-1} \text{ sr}^{-1} M_\odot^{-1}$; and $t_{z, z'}$ is the time elapsed between redshifts z' and z . The time dependence of $j(\nu)$ is obtained from our fitted light-curve function $f(t)$ in equation (2) for quasars, and from tabulated evolutionary tracks for stars (Schaller et al. 1992; see HL97 for details). We suppressed the emergent flux from all objects at emission frequencies above $\text{Ly}\alpha$ before reionization occurs (assuming sudden reionization at the redshift $z = 13$ or 9 for stars, and $z = 11.5$ for quasars), since the Gunn–Peterson optical depth of HI at these frequencies is exceedingly high prior to reionization.

Figure 9 shows the predicted number counts normalized to the field of view of SIRTf (which is scheduled for launch long before NGST), $5' \times 5'$; the planned field-of-view of NGST is similar, $4' \times 4'$. Figure 9 shows separately the number per logarithmic flux interval of all objects with $z > 5$ (thin lines), and with $z > 10$ (thick lines). In general, the number of detectable sources is high. With its expected sensitivity, NGST will be able to probe about 10^3 quasars at $z > 10$, and $10^{3.5}$ quasars at $z > 5$ (solid curves) per field of view. The bright-end tail of the number

counts approximately follows the power law $dN/dF_\nu \propto F_\nu^{-2.5}$. This slope is too shallow for foreground galaxies to significantly increase the number counts due to the amplification bias from gravitational lensing. The top solid curve also shows that the number of faint quasars starts to turn over below ~ 1 nJy, as a result of the cutoff in the minimum halo mass that allows atomic line cooling. The average angular separation between the quasars at $z > 10$ would be $\sim 10''$, well above the angular resolution limit of $0.06''$ planned for NGST. For comparison, we show in Figure 9 the corresponding number counts of “star-clusters”, i.e. assuming that each halo shines due to a starburst that converts a fraction 0.017-0.17 of the gas into stars. The dashed lines indicate that NGST might detect $10^{1.5}$ – $10^{3.5}$ star-clusters at $z > 10$ per field of view, and $10^{3.5}$ – $10^{4.5}$ clusters at $z > 5$. Unlike quasars, star clusters could in principle be resolved, if they extend over a scale comparable to the virial radius of the collapsed halo (Haiman & Loeb 1997b).

6. Conclusions

We extrapolated the quasar luminosity function to faint magnitudes and high redshifts, based on the assumptions that the halo formation rate follows the Press-Schechter theory, and that the quasar light-curve scales linearly with the halo mass, and is otherwise a universal function of time. We demonstrated that a universal light-curve of the form, $L(t) = L_{\text{Edd}} \exp(-t/t_0)$, with $t_0 = 6.6 \times 10^5$ yr and L_{Edd} being the Eddington luminosity, provides an excellent fit to observational data for the quasar LF between $2.6 < z < 4.5$ provided that the final black hole mass is a fraction $\sim 5.4 \times 10^{-3}$ of the baryonic mass in each object. This fraction is surprisingly close to the roughly universal ratio between black hole and bulge masses observed in nearby galaxies (Magorrian et al. 1997). Our extrapolation of the quasar LF to high redshifts and low luminosities as presented in Figure 4, can be viewed as a natural by-product of this physically motivated fit.

Given the Press-Schechter prediction for the formation rate of halos, and the fact that t_0 is much shorter than the Hubble time, our prediction for the reionization history depends only on the integral of the inferred light-curve, namely on the mean radiative efficiency of the material that made the black hole. The low value inferred for t_0 implies an average radiative efficiency of only $\sim 0.1\%$. This rather low estimate for the efficiency is smaller by two orders of magnitude than the value expected in thin disk accretion; any increase in its value would only enhance the effects we predict. Despite our conservative approach, we predict an extensive population of faint quasars at high redshifts. For illustration, we show in Figure 5 the expected evolution in the number density of bright quasars with absolute B magnitude $M_B < -27.5$, along with that of quasars which are two orders of magnitude fainter. Although the density of bright quasars in our models declines rapidly beyond redshift $z \sim 3$ in good agreement with existing observations at $2.6 < z < 4.5$, we predict an abundant population of faint quasars which extends out to redshifts $z \gtrsim 10$, and has not yet been directly observed.

We find that, in general, the effects of early quasars are comparable to those of early stars. However, stellar effects scale with the average IGM metallicity that we used to normalize the star

formation efficiency. If the observed values of the C/H ratio in the individual Ly α forest clouds are representative of the universal average C/H ratio, than this ratio implies an IGM metallicity of $\sim 0.5\text{--}1\%$ solar. However, if the overall carbon abundance is patchy, because it is not well mixed with the rest of the intergalactic gas (as argued by Gnedin 1997), then the true average metallicity may be an order of magnitude lower, 0.1% solar (Songaila 1997). We have found that at the high end of the allowed metallicity range, the effects of stars are stronger than that of quasars, while at the low end of this range, quasars are more effective. In particular, quasars reionize the universe at $z \sim 11.5$, while stars at $9 \lesssim z \lesssim 13$. The Compton y -parameter for the spectral distortion of the CMB is expected to be $1.3 \times 10^{-7} < y_c < 1.2 \times 10^{-5}$ from starlight alone, and $4.1 \times 10^{-6} < y_c < 2.0 \times 10^{-5}$ if the flux of quasars is added. The direct far-infrared flux from quasars yields a lower limit to the distortion, $y_c \gtrsim 3.4 \times 10^{-6}$, even in the absence of any intergalactic dust. The expected number of $z > 10$ quasars per square arcminute, brighter than 1nJy in the wavelength range $1\text{--}3.5\mu\text{m}$, is ~ 40 , while the corresponding number for star clusters is $\sim 1\text{--}100$. Both of these numbers are large enough to show as a distinct population on a typical image by the forthcoming Next Generation Space Telescope.

We thank J. McDowell, Y. Pei, and W. Zheng for data on quasar spectra and the quasar luminosity function, and L. Hui, J. Miralda-Escudé, R. Narayan, M. Rees, E. Turner, and A. Songaila for useful discussions. This work was supported in part by the NASA ATP grant NAG5-3085, and the Harvard Milton fund.

REFERENCES

- Adams, F. C., Freese, K., Levin, J., McDowell, J. 1989, *ApJ*, 344, 24
- Bechtold, J. 1994, *ApJS*, 91, 1
- Bennett, C. L., Banday, A. J., Gorski, K. M., Hinshaw, G., Jackson, P., Keegstra, P., Kogut, A., Smoot, G. F., Wilkinson, D. T., & Wright, E. L. 1996, *ApJ*, 464, L1
- Bond, J. R. 1995, in *Theory and Observations of the Cosmic Microwave Background Radiation*, ed. Schaeffer, R. (Elsevier: Netherlands), in press
- Bond, J. R., Cole, S., Efstathiou, G. & Kaiser, N. 1991, *ApJ*, 379, 440
- Bond, J. R., Carr, B. J., & Hogan, C. J. 1991, *ApJ*, 367, 420
- Boyle, B. J., Jones, L. R., Shanks, T., Marano, B., Zitelli, V., & Zamorani, G. 1991, in Crampton, D., ed., *ASP Conf. Series No. 21, The Space Distribution of Quasars*, Astron. Soc. Pacif., San Francisco, p. 191
- Carlberg, R. G. 1990, *ApJ*, 350, 505
- Carr, B. J., Bond, J. R., & Arnett, W. D. 1984, *ApJ*, 277, 445
- Carroll, S. M., Press, W. H., Turner, E. L. 1992, *ARA&A*, 30, 499

- Davidson, A. F., Kriss, G. A., Zheng, W. 1996, *Nature*, 380, 47
- Draine, B. T., & Lee, H. M. 1984, *ApJ*, 285, 89
- Efstathiou, G., & Bond, J. R. 1987, *MNRAS*, 227, 33p
- Efstathiou, G., & Rees, M. J. 1988, *MNRAS*, 230, 5p
- Eisenstein, D. J. 1997, *ApJ*, submitted, preprint astro-ph/9709054
- Eisenstein, D.J., & Loeb, A. 1995, *ApJ*, 443, 11
- Elvis, M., Wilkes, B. J., McDowell, J. C., Green, R. F., Bechtold, J., Willner, S. P., Oey, M. S., Polomski, E., & Cutri, R. 1994, *ApJS*, 95, 1
- Fixsen, D. J., Cheng, E. S., Gales, J. M., Mather, J. C., Shafer, R. A., Wright, E. L. 1996, *ApJ*, 473, 576
- Frank, J., King, A., & Raine, D. 1992, *Accretion Power in Astrophysics* (Cambridge: Cambridge Univ. Press)
- Franx, M, Illingworth, G. D., Kelson, D. D., van Dokkum, P. G., & Tran, K.-V. 1997, *ApJ*, 486, L75
- Giroux, M. L., & Shull, J. M. 1997, *AJ*, 113, 1505
- Gnedin, N. Y., *MNRAS*, in press, preprint astro-ph/9709224
- Gnedin, N. Y., & Ostriker, J. P. 1997, *ApJ*, 486, 581
- Haiman, Z., & Loeb, A. 1997a, *ApJ*, 483, 21 (HL97)
- 1997b, to appear in the Proceedings of Science with the Next Generation Space Telescope (Eds. E. Smith & A. Koreans), astro-ph/9705144
- Haiman, Z., Rees, M. J., & Loeb, A. 1996, *ApJ*, 467, 522
- 1997, *ApJ*, 476, 458
- Haiman, Z., Thoul, A., & Loeb, A. 1996, *ApJ*, 464, 523
- Haehnelt, M. G., & Rees, M. J. 1993, *MNRAS*, 263, 168
- Hogan, C. J., Anderson, S. F., Rugers, M. H. 1997, *AJ*, 113, 1495
- Hu, W., & White, M. 1997, *ApJ*, 479, 568
- Jacobsen, P., Boksenberg, A., Deharveng, J. M., Greenfield, P., Jedrzejewski, R., & Paresce, F. 1994, *Nature*, 370, 35
- Kamionkowski, M., Spergel, D. N., & Sugiyama, N. 1994, *ApJL*, 426, L57
- Kormendy, J., Bender, R., Magorrian, J., Tremaine, S., Gebhardt, K., Richstone, D., Dressler, A., Faber, S. M., Grillmair, C., & Lauer, T. R. 1997, *ApJ*, 482, L139
- Lacey, C. G., & Cole, S. 1993, *MNRAS*, 262, 627
- 1994, *MNRAS*, 271, 676

- Loeb, A. 1997, “The First Stars and Quasars in the Universe”, to appear in Proc. of “Science with the Next Generation Space Telescope”, April 1997, preprint astro-ph/9704290
- Loeb, A., & Haiman, Z. 1997, ApJ, 490, in press, preprint astro-ph/9704133 (LH97)
- Magorrian, J., et al. 1997, submitted to ApJ, preprint astro-ph/9708072
- Madau, P., & Meiksin, A. 1994, ApJ, 433, L53
- Mather, J., & Stockman, P. 1996, STSci Newsletter, v. 13, no. 2, p. 15
- Mathis, J. S. 1990, ARA&A, 28, 37
- McLeod, K. 1996, in ESO-IAC conference on Quasar Hosts, Tenerife, in press
- Miralda-Escudé, J. 1997, ApJ, in press, preprint astro-ph/9708253
- Miralda-Escudé, J., & Rees, M. J. 1994, MNRAS, 266, 343
- 1997, ApJ, 478, L57
- Narayan, R. 1996, “Advective Disks”, to appear in Proc. IAU Colloq. 163 on Accretion Phenomena & Related Outflows, A.S.P. Conf. Series, eds. D. T. Wickramasinghe, L. Ferrario, G. V. Bicknell, in press, preprint astro-ph/9611113
- Ostriker, J. P., & Steinhardt, P. J. 1995, Nature, 377, 600
- Pei, Y. C. 1995, ApJ, 438, 623
- Press, W. H., & Schechter, P. L. 1974, ApJ, 181, 425
- Rees, M. J. 1996, preprint astro-ph/9608196
- Reimers, D., Köhler, S., Wisotzki, L., Groote, D., Rodriguez-Pascual, P., & Wamsteker, W. 1997, A&A, in press, preprint astro-ph/9707173
- Sasaki, S. 1994, PASJ, 46, 427
- Scalo, J. M. 1986, Fundamentals of Cosmic Physics, vol. 11, p. 1-278
- Schaller, G., Schaerer, D., Meynet, G., & Maeder, A. 1992, A&ASS, 96, 269
- Schneider, D. P., Schmidt, M., & Gunn 1991, J. E, AJ, 102, 837
- Scott, D., Silk, J., & White, M. 1995, Science, 268, 829
- Shapiro, P. R., & Giroux, M. L. 1987, ApJ, 321, L107
- Small, T. A., & Blandford, R. D. 1992, MNRAS, 259, 725
- Songaila, A. 1997, ApJL, in press, preprint astro-ph/9709046
- Songaila, A., & Cowie, L. L. 1996, AJ, 112, 335
- Tytler, D. et al. 1995, in QSO Absorption Lines, ESO Astrophysics Symposia, ed. G. Meylan (Heidelberg: Springer), p.289
- van der Marel, R. de Zeeuw, P. T., Rix, H-W., & Quinlan, G. D. 1997, Nature, 385, 610
- Wright, E. L. 1981, ApJ, 250, 1

Wright, E. L., et al. 1994, ApJ, 420, 450

Yi, I. 1996, ApJ, 473, 645

Zaldarriaga, M., Spergel, D., & Seljak, U. 1997, preprint astro-ph/9702157

Zheng, W., Kriss, G. A., Telfer, R. C., Grimes, J. P., Davidsen, A. F. 1997, ApJ, 475, 469

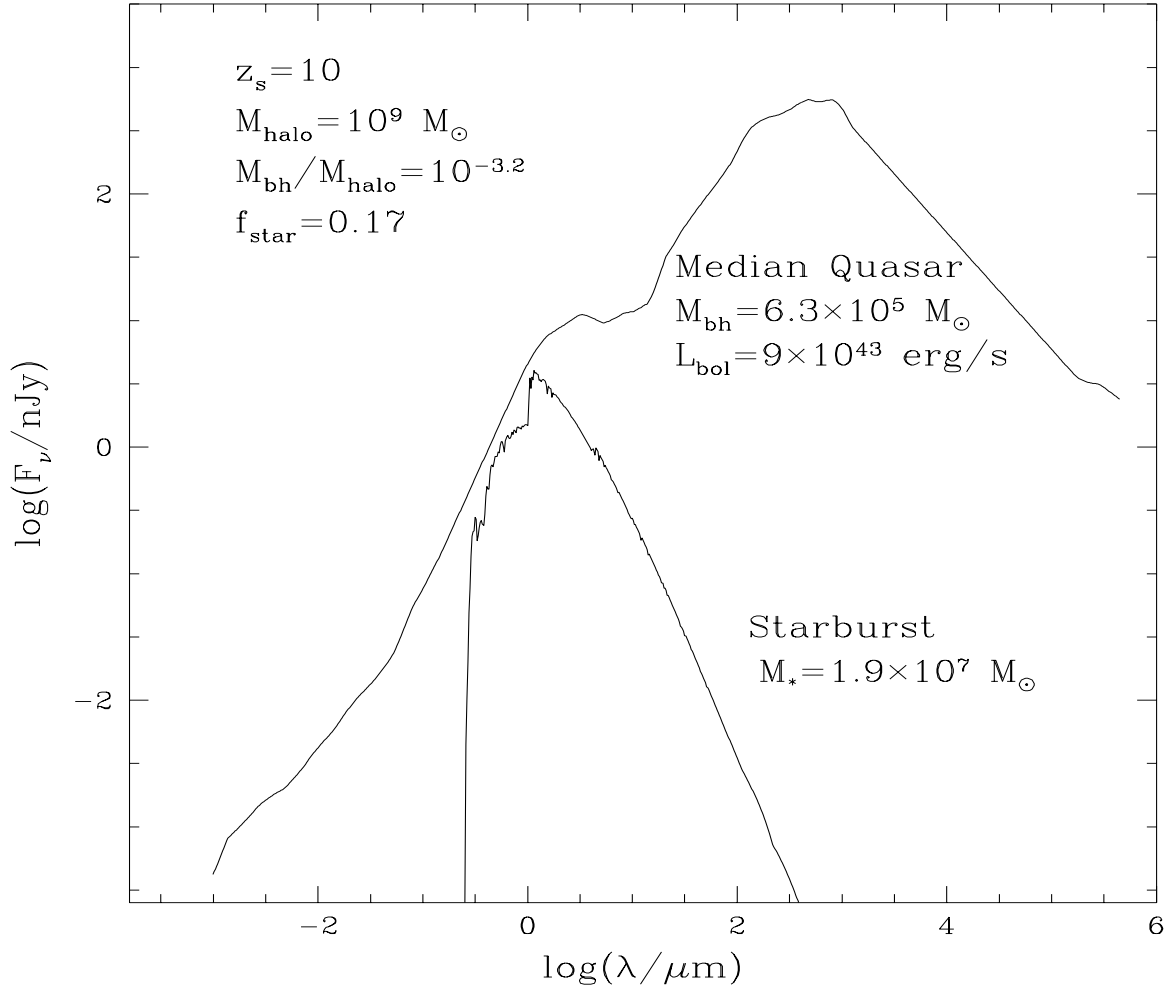


Fig. 1.— Comparison of the observed spectral fluxes from a typical quasar and a starburst in a source located at redshift $z_s = 10$. The star-formation efficiency, $f_{\text{star}} = 0.17$, was fixed so as to produce an average of 1% solar metallicity in the IGM at $z = 3$. The black hole formation efficiency, $M_{\text{bh}}/M_{\text{halo}} = 10^{-3.2}$, was found by our fitting procedure to the observed quasar luminosity function (see text for details).

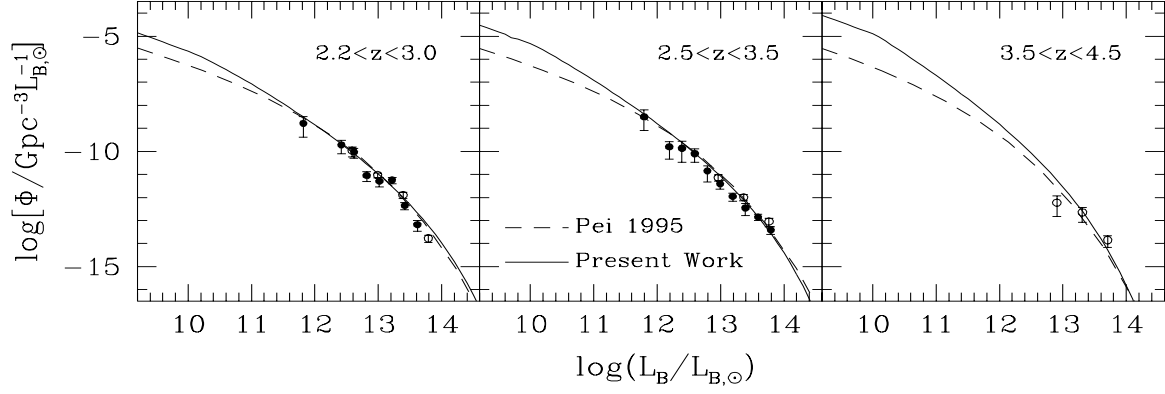


Fig. 2.— The observed and extrapolated evolution of the quasar luminosity function in a Λ CDM cosmology. The data is taken from Pei (1995), and the dashed lines show the parametric fitting function from this reference. The solid lines show our fits based on the Press–Schechter formalism and the universal light–curve shown in Fig. 3.

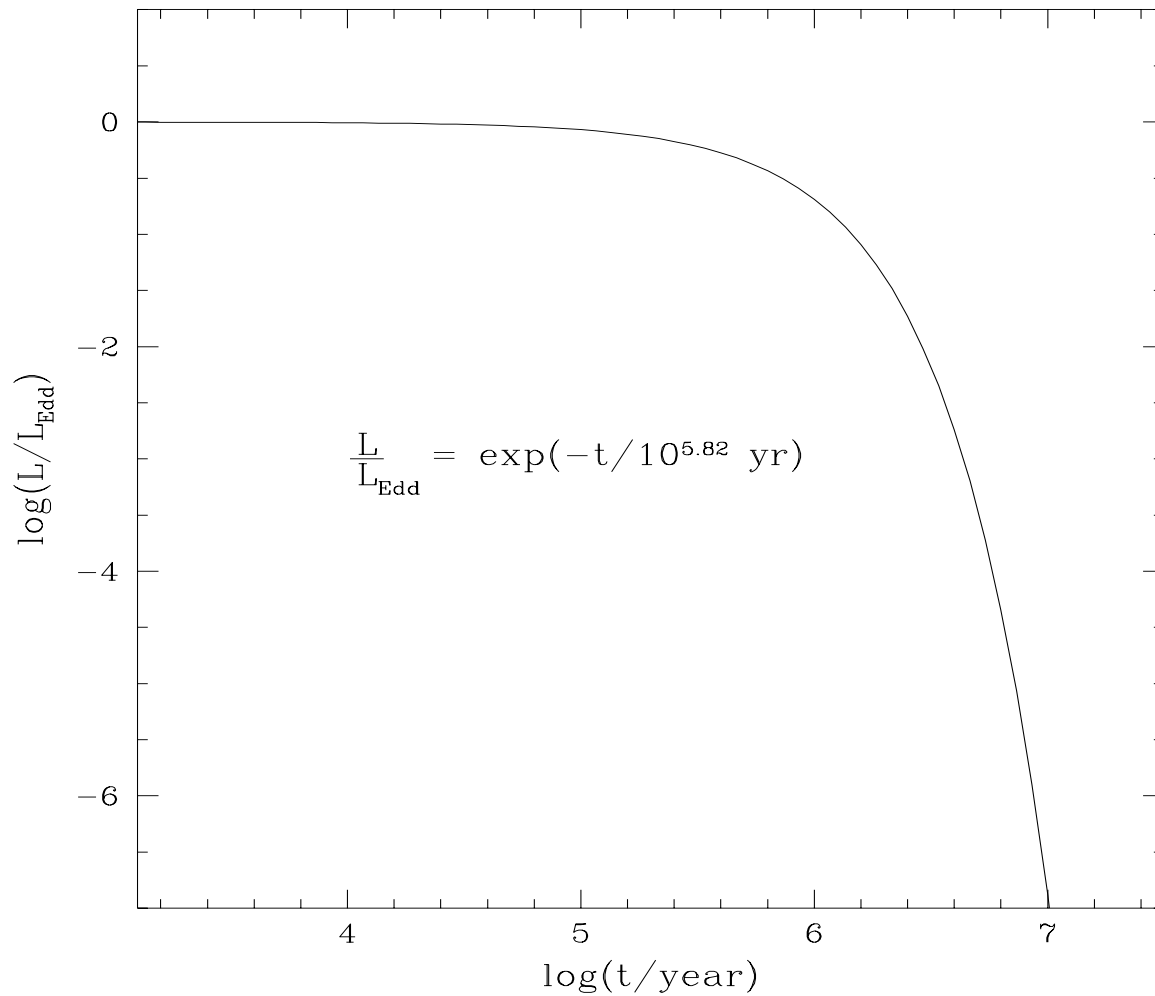


Fig. 3.— The best-fit quasar light-curve in Eddington units, that results in the luminosity functions shown by the solid lines in Figure 2. The Eddington time was not used to rescale the time axis, because it does not depend on the black hole mass, and is a constant for a universal radiative efficiency.

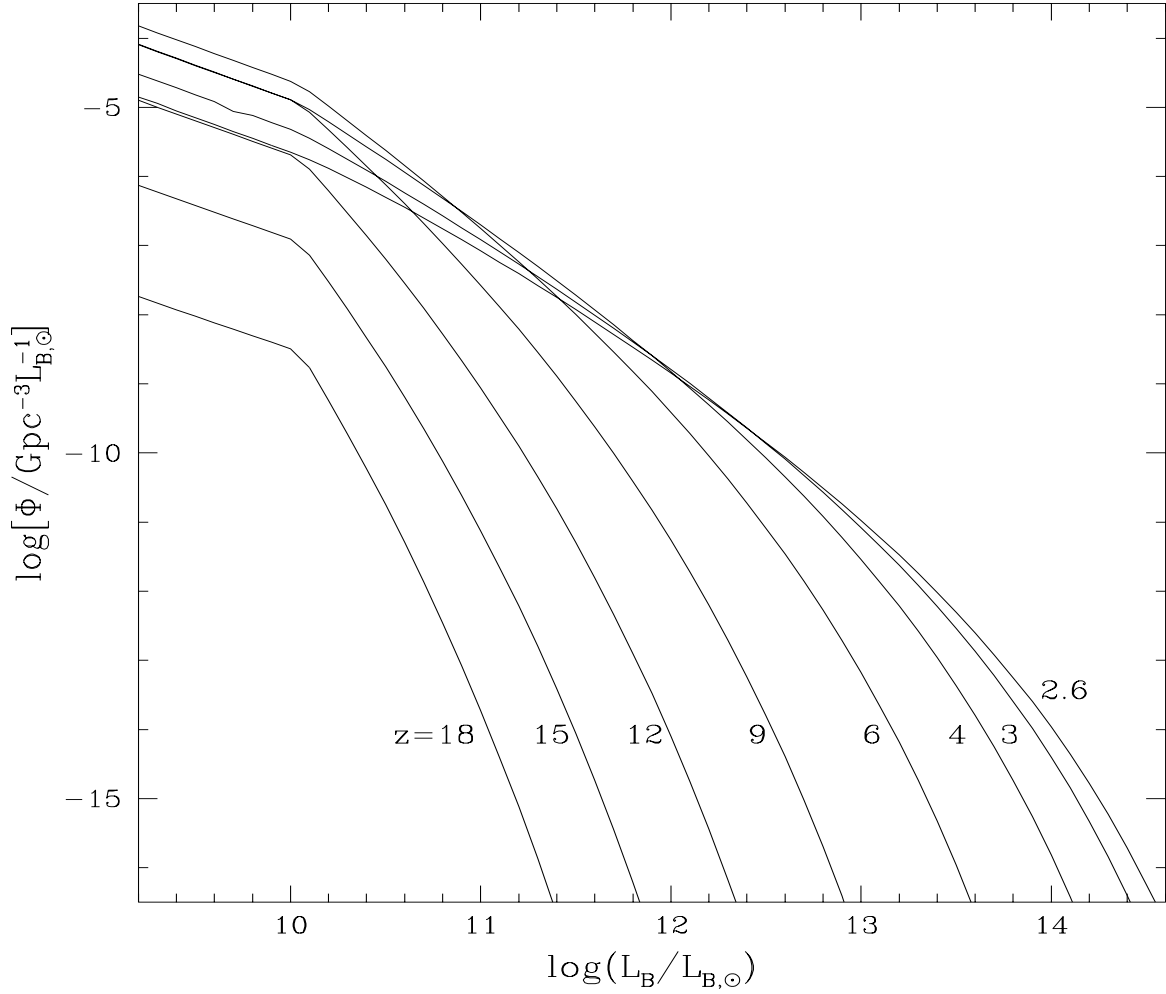


Fig. 4.— The extrapolated quasar luminosity function at high redshifts, using the light–curve of Figure 3. The break at $L_B \sim 10^{10} L_{B,\odot}$ is a result of the low mass cutoff for the dark matter halo, $M_{\min} = 10^8 M_\odot [(1+z)/10]^{-3/2}$, that defines the threshold for efficient (atomic) cooling of virialized gas.

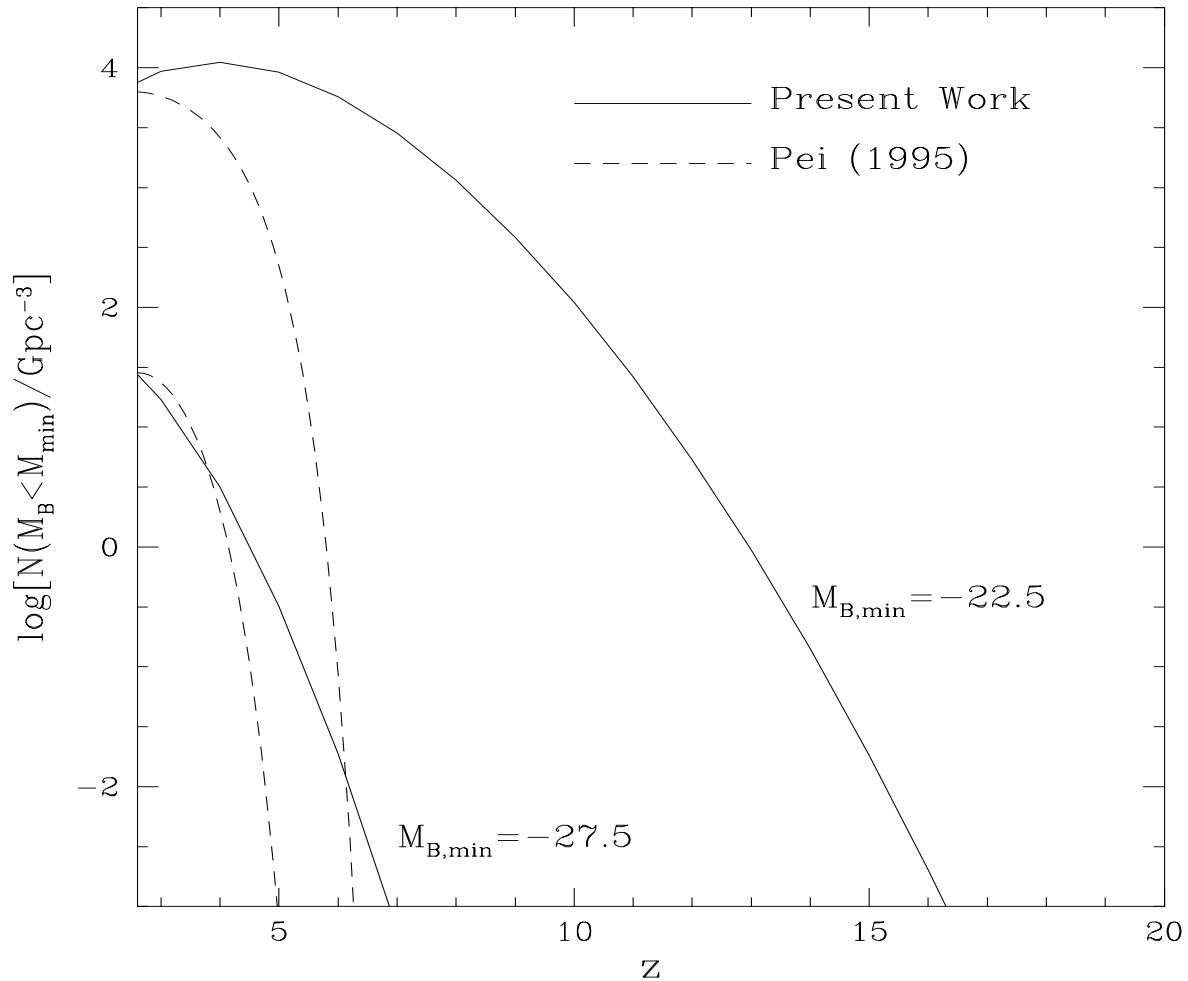


Fig. 5.— The redshift evolution of the number density of quasars. Solid lines show the predictions from our model, while the dashed lines show the formal extrapolation of the fitting formulae obtained by Pei (1995).

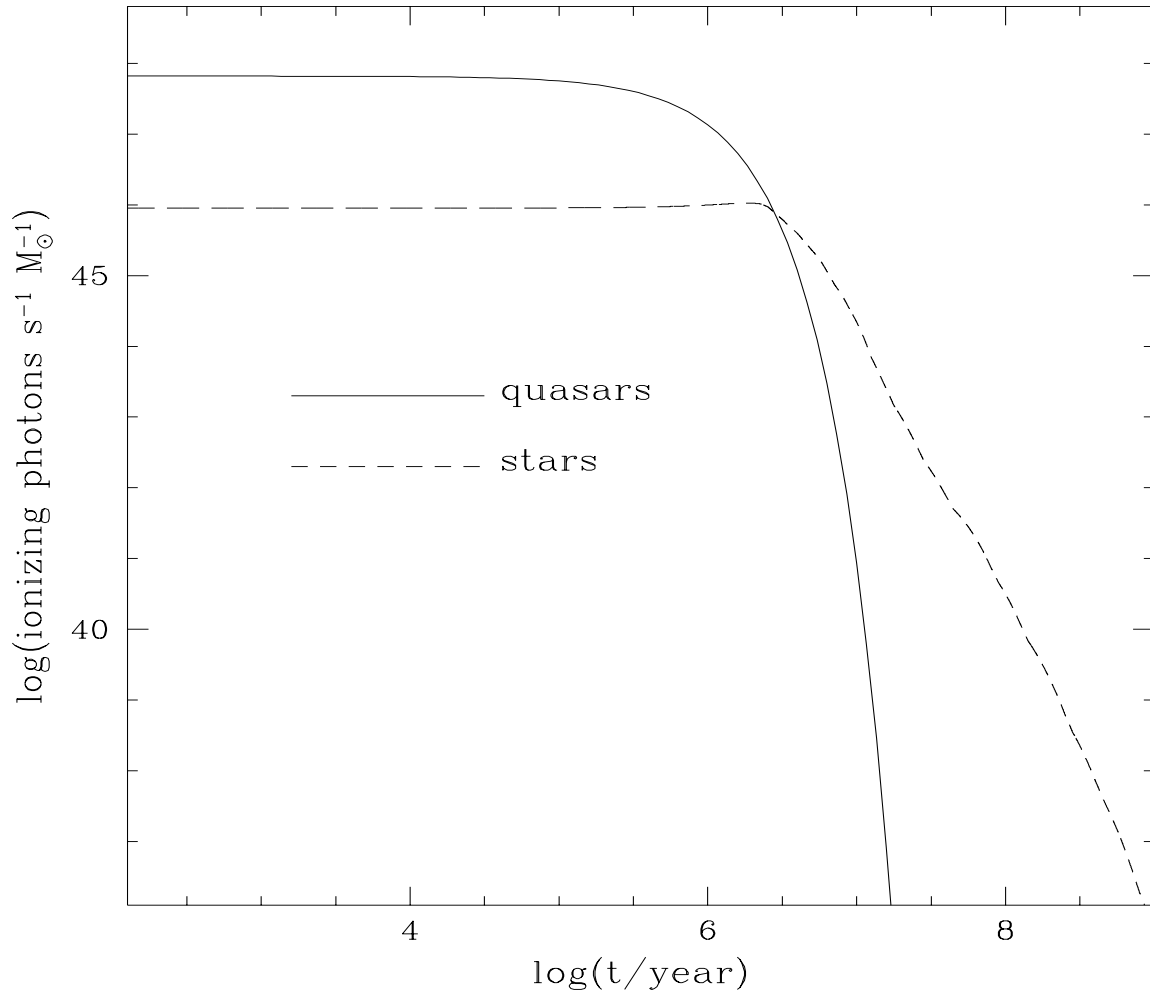


Fig. 6.— Evolution of the production rate of ionizing photons, per unit black hole mass in quasars (solid curve), and per unit stellar mass in a starburst (dashed curve).

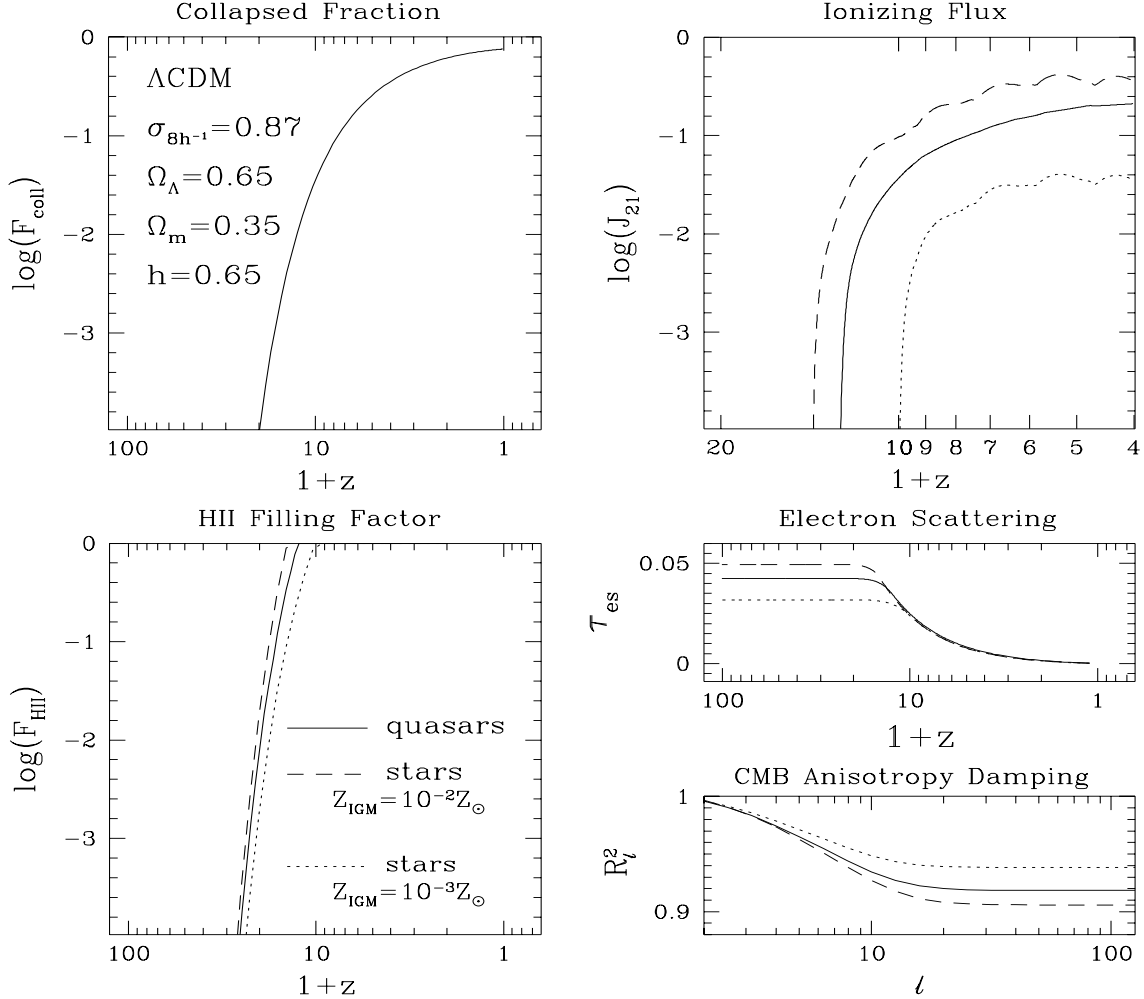


Fig. 7.— Reionization history from quasars (solid lines) and early stars (dashed [$Z_{\text{IGM}} = 10^{-2}Z_{\odot}$] and dotted [$Z_{\text{IGM}} = 10^{-3}Z_{\odot}$] lines). The different panels show (i) the collapsed fraction of baryons; (ii) the evolution of the flux at the local Lyman limit frequency, in units of $10^{-21} \text{ erg s}^{-1} \text{ cm}^{-2} \text{ Hz}^{-1} \text{ sr}^{-1}$; (iii) the volume filling factor of ionized regions; and (iv) the optical depth to electron scattering, τ_{es} , and the corresponding damping factor, R_{ℓ}^2 , for the power-spectrum decomposition of CMB anisotropies as a function of the spherical harmonic index ℓ .

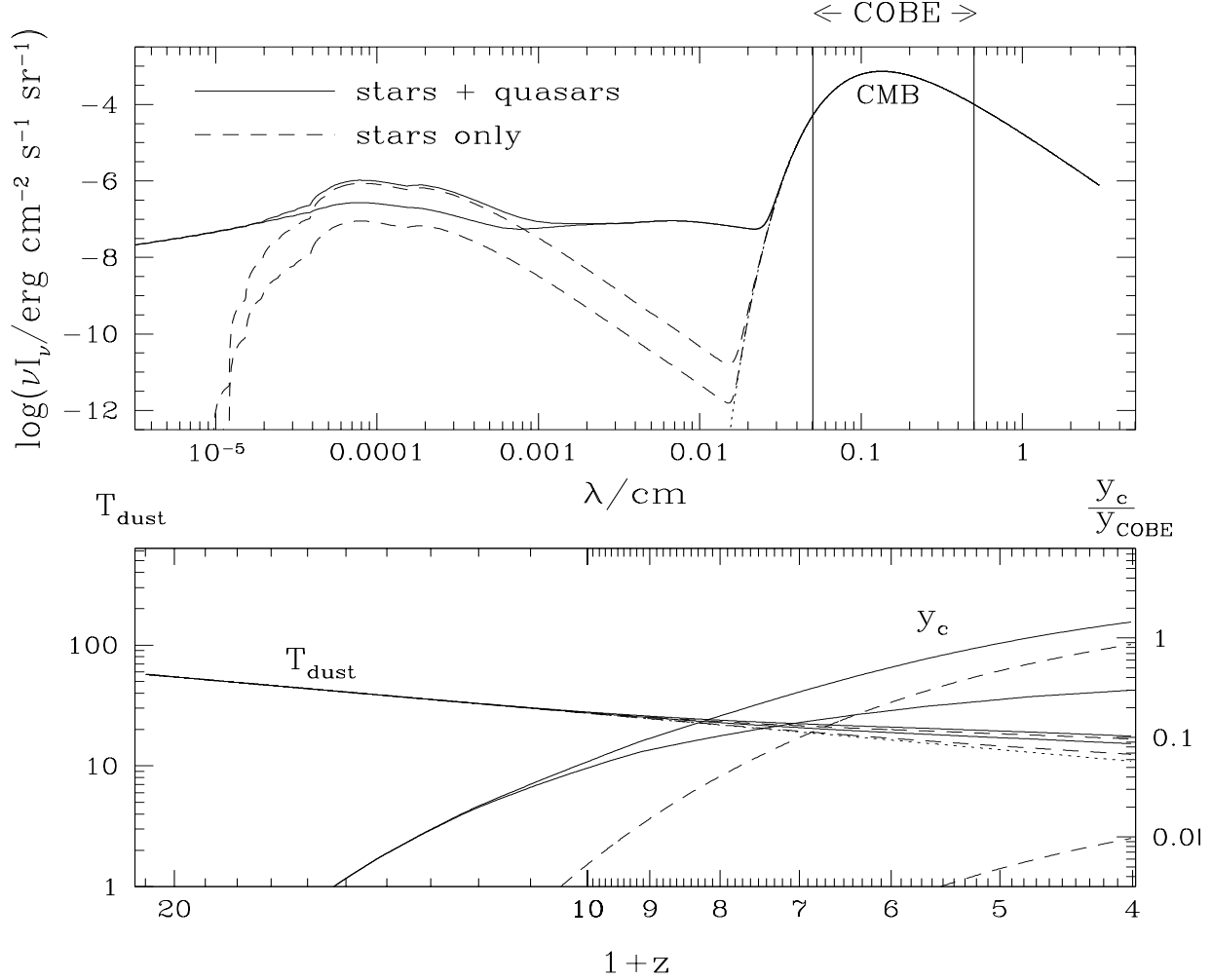


Fig. 8.— Upper panel: The full (CMB + direct light + dust emission) background flux at redshift $z = 3$ in the presence of early stars alone (dashed lines) and in the presence of both stars and quasars (solid lines). The pairs of dashed and solid lines bracket the possible range of the IGM metallicity, $10^{-3}Z_\odot < Z_{\text{IGM}} < 10^{-2}Z_\odot$. Lower panel: The corresponding redshift evolution of the dust temperature, and the Compton y -parameter. The dotted curve shows the CMB temperature, $T_{\text{CMB}} = 2.728(1+z)\text{K}$.

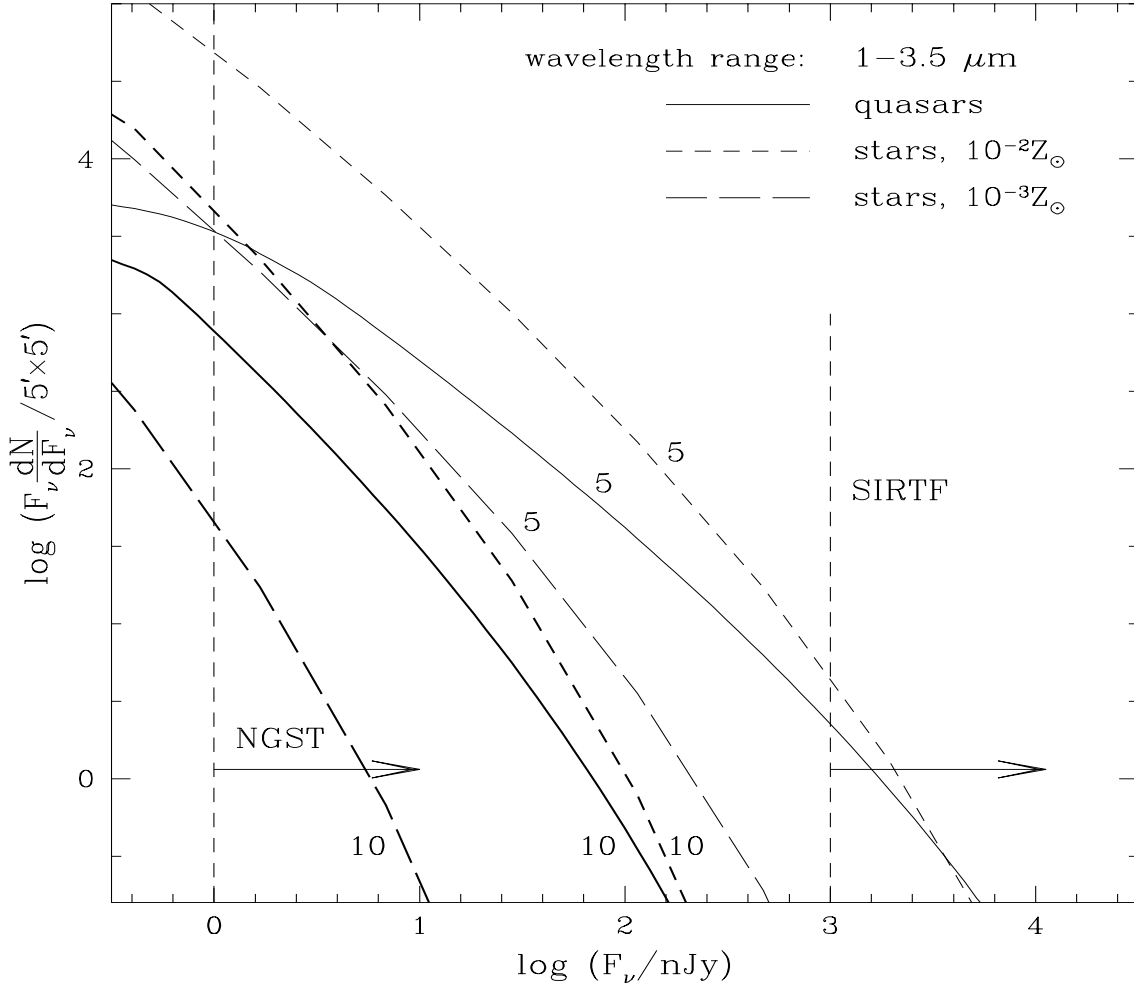


Fig. 9.— The number per logarithmic flux interval of high-redshift objects which could be probed by future space telescopes, in the wavelength range of $1\text{--}3.5\mu\text{m}$. We assume sudden reionization at $z=11.5$ for quasars, and at $z=9$ or 13 for stars. The vertical dashed lines show the expected sensitivities of the Space Infrared Telescope Facility (SIRTf) and the Next Generation Space Telescope (NGST). The thick lines, labeled “10”, correspond to objects located at redshifts $z > 10$, and the thin lines, labeled “5”, correspond to objects located at redshifts $z > 5$.